

Nucleosomes enter cells by clathrin- and caveolin-dependent endocytosis

Huawei Wang, Xiajing Shan, Mengtian Ren, Mengdi Shang and Chuanzheng Zhou^{✉*}

State Key Laboratory of Elemento-Organic Chemistry and Department of Chemical Biology, College of Chemistry, Nankai University, Tianjin 300071, China

Received July 28, 2021; Revised October 20, 2021; Editorial Decision October 23, 2021; Accepted October 25, 2021

ABSTRACT

DNA damage and apoptosis lead to the release of free nucleosomes—the basic structural repeating units of chromatin—into the blood circulation system. We recently reported that free nucleosomes that enter the cytoplasm of mammalian cells trigger immune responses by activating cGMP-AMP synthase (cGAS). In the present study, we designed experiments to reveal the mechanism of nucleosome uptake by human cells. We showed that nucleosomes are first absorbed on the cell membrane through non-specific electrostatic interactions between positively charged histone N-terminal tails and ligands on the cell surface, followed by internalization via clathrin- or caveolae-dependent endocytosis. After cellular internalization, endosomal escape occurs rapidly, and nucleosomes are released into the cytosol, maintaining structural integrity for an extended period. The efficient endocytosis of extracellular nucleosomes suggests that circulating nucleosomes may lead to cellular disorders as well as immunostimulation, and thus, the biological effects exerted by endocytic nucleosomes should be addressed in the future.

INTRODUCTION

In eukaryotic cells, genomic DNA is packed as chromatin, of which nucleosomes are the basic structural repeating units. A nucleosome is composed of a double-stranded (dsDNA) fragment wrapped around a histone octamer (each with two H2A, H2B, H3 and H4 histones) (1). Under certain pathological conditions, especially during apoptosis, chromatin fragments leading to the release of nucleosomes into the blood circulation system (2–4). Increased levels of circulating nucleosomes are observed in patients with autoimmune disease, which has generated interest in revealing the linkage between nucleosomes and immunostimulation (5). Recently, a few research groups reported that nucleosomes can bind cGMP-AMP synthase (cGAS) (6–12), a cytoplasmic pattern-recognition receptor

of the mammalian innate immune system (13,14). Nucleosome binding stimulates cGAS to synthesize the second messenger 2',5'-cyclic GMP-AMP (cGAMP). Although nucleosome-bound cGAS shows reduced activity compared with dsDNA-bound cGAS (6,7), these studies revealed a potential pathway for the immunogenicity of circulating nucleosomes.

To bind cGAS and trigger the immune response in the cytoplasm, extracellular nucleosomes must be transported across the plasma membrane, which protects intracellular components against the extracellular environment. Oligonucleotides and dsDNA fragments, due to their negative charge and hydrophilic features, cannot easily enter cells (15,16). In contrast, Lys- and Arg-rich histones are positively charged small proteins that can be efficiently taken up by mammalian cells (17,18). Complexing anionic DNA with cationic polymers to form nanoparticles is an advanced strategy for inducing cellular uptake of DNA (19). Nucleosomes themselves are DNA–histone complexes and form zwitterionic nanoparticles. We thus argue that these physicochemical features may allow nucleosomes to be directly taken up by mammalian cells. To this end, we have demonstrated that extracellular nucleosomes can be taken up by different types of mammalian cells, and after cellular entry, these nucleosomes trigger innate immune responses via cGAS activation in the cytosol (20). In the present study, we designed experiments to address the mechanism of cellular internalization of nucleosomes. We found that nucleosomes enter human cells mainly by clathrin- and caveolin-dependent endocytic pathways, and after endocytosis, these structures escape quickly from endosomes and remain intact for an extended period in the cytosol.

MATERIALS AND METHODS

Materials and general methods

Dynasore and genistin (GE) were obtained from Aladdin (Shanghai, China). Methyl- β -cyclodextrin (M β CD) was purchased from TCI (Shanghai, China). Sucrose was purchased from Meilun Biological (Dalian, China). Opti-MEM (minimum essential media) was purchased from Invitrogen (MA, USA). ER (endoplasmic reticulum)-Tracker

*To whom correspondence should be addressed. Tel: +86 22 23497531; Fax: +86 22 23497531; Email: chuanzheng.zhou@nankai.edu.cn

Red, Golgi-Tracker Red, Lyso-Tracker Red and Western Lightning BeyoECL Plus were obtained from Beyotime (Shanghai, China). An anti-EEA1 (early endosome antigen 1) mouse monoclonal antibody and horseradish peroxidase-conjugated secondary antibody directed against rabbit IgG, β -actin and caveolin-1 rabbit polyclonal antibody were purchased from Proteintech (Wuhan, China). Clathrin heavy chain (CHC) rabbit pAb was purchased from ABclonal (Wuhan, China). DyLight 649 goat anti-mouse IgG (H + L) was purchased from Abbkine (California, USA). DAPI, RIPA buffer and 5% BSA were purchased from Solarbio (Beijing, China). Histone mutants (Supplementary Table S1) were expressed in *Escherichia coli* strain BL21 (DE3) as previously described (21).

Cell culture

HeLa cells were cultured in Dulbecco's modified Eagle's medium (DMEM; Gibco) with 10% fetal bovine serum (FBS) and 100 U/ml penicillin streptomycin (Invitrogen) at 37°C and 5% CO₂. THP-1 cells were cultured in RPMI-1640 (Gibco) containing 10% FBS, 50 U/ml penicillin, 50 μ g/ml streptomycin, 2 mM L-glutamine and 50 μ M β -mercaptoethanol at 37°C in 5% CO₂.

Reconstitution of nucleosomes

The general procedure for preparing FAM-145 nucleosomes was described previously (20). Briefly, dsDNA molecules were prepared by PCR amplification. After PCR amplification, dsDNA was purified by 1.5% agarose gel electrophoresis. The target bands were excised from the gel and purified by a gel extraction kit (Tianmobio, Beijing, China). dsDNA (100 pmol) and histone octamer (130 pmol) were combined in a Slide-A-Lyzer MINI Dialysis Unit (3500 MWCO, Thermo Scientific) to a final volume of 100 μ l containing 2 M NaCl. The dialysis unit was then placed inside another dialysis bag filled with ~20 ml of buffer (2 M NaCl, 10 mM HEPES pH 7.5, 1 mM EDTA). This bag was then placed in 2 l of low-salt buffer (10 mM HEPES, pH 7.5, 1 mM EDTA) and left to dialyze overnight at 4°C. The sample was incubated at 37°C for 2 h, and any precipitate was pelleted via a brief (10 min) centrifugation at 7000 g. The solution was then transferred to a fresh siliconized tube, and the concentration of nucleosomes was determined based on the A_{260} of dsDNA. A small aliquot was removed and analysed by 1.5% agarose gel electrophoresis for 30 min at 150 V in 0.2 \times TBE (Supplementary Figure S1).

Cy3 labelling of nucleosomes

For labelling of the FAM-145 nucleosomes with Cy3, 0.6 μ l of Cy3-NHS (0.26 mM) was added to a solution of FAM-145 nucleosomes (0.2 μ M, 50 μ l). The reaction mixture was incubated at 35°C for 2 h. Excess Cy3-NHS was removed by PD SpinTrap G-25 according to the manufacturer's instructions. The structural integrity of the obtained FAM-Cy3-145 nucleosomes was analysed by 1.5% agarose gel electrophoresis performed for 30 min at 150 V in 0.2 \times TBE.

DNase I footprinting of nucleosomes

FAM-145-nucleosomes or FAM-Cy3-145-nucleosomes (16 μ l each) were mixed with 2 μ l of 10 \times DNase I buffer and treated with various amounts of DNase I (total ~20 μ l) for 3 min at room temperature. The reaction was terminated by heating at 95°C. Then, the sample was chilled on the ice. The sample was digested with 2 μ l of proteinase K (5 mg/ml). The obtained samples were analysed by 20% denaturing PAGE (40 \times 32 \times 0.04 cm, run under limiting power (50 W) until the bromophenol blue band migrated to the bottom).

Flow cytometry

HeLa cells were grown until 70–80% confluence in 48- or 24-well tissue culture plates. Each well was incubated with nucleosomes (20 nM). The cells were then detached by trypsin, washed with serum-rich DMEM to neutralize trypsin activity, and resuspended in 330–500 μ l of PBS. The samples were immediately analysed by flow cytometry (BD, USA). BD LSRFortessa was used for acquisition, and FlowJo V10 was used for data analysis. Mean fluorescence intensity (MFI) is an average linear value for events in the defined population, defined as: $\bar{X} = (\sum_{i=1}^n X_i)/n$, where n = number of events in the population, and X_i is a value for a particular parameter, where $i = 1$ to n . For THP-1, cells were harvested and washed with an acidic solution (0.5 M NaCl, 0.5% acetic acid, pH 3.0) before flow cytometry analysis.

Absorption assays

HeLa cells were seeded in 48-well plates. After overnight culture on glass coverslips, the cells were incubated at 4°C for 30 min. FAM-labelled nucleosomes (40 nM) were added, followed by incubation for 30 min at 4°C. After the cells were washed with PBS, they were fixed in 4% paraformaldehyde (PFA) for 15 min at room temperature. The fixed cells were washed in PBS and stained with DAPI, and coverslips were mounted onto clean glass slides. Image capture was performed by laser scanning confocal microscopy (LSCM) using an Olympus FV1000S-IX81 LSC microscope.

For trypsin treatment, the cells were treated with trypsin for 1 min at 37°C, the trypsin was removed, and fresh medium was added. After incubation at 4°C for 30 min, FAM-labelled nucleosomes (40 nM) were added, followed by incubation for 30 min at 4°C. The rest of the procedure was the same as that described above.

For acid treatment, the cells were incubated at 4°C for 30 min. FAM-labeled nucleosomes (40 nM) were added, followed by incubation for 30 min at 4°C. Then, the cells were washed by acidic solution (0.5 M NaCl, 0.5% acetic acid, pH 3.0) twice. The rest of the operation was the same as that described above.

Chemical inhibition assays

HeLa cells were grown in 48-well tissue culture plates. After the cell medium was changed to Opti-MEM, endocytosis inhibitors, including dynasore (80 μ M), GE (200 μ M),

M β CD (2 mM), sucrose (45 mM), NaN₃ (0.1%) or EIPA (100 mM), were added to the medium and incubated for 1 h at 37°C. Then, the medium was changed to fresh media containing the inhibitors (except EIPA) plus 145-FAM-nucleosomes (20 nM), and incubation was continued for 6 h at 37°C/5% CO₂. The treated cells were analysed by flow cytometry as described above.

siRNA inhibition assays

The small interfering RNA 5'-AGACGAGCUGAGCGAGAAGdTdT-3' for knocking down caveolin-1 (siCAV), siRNA 5'-UAAUCCAAUUCGAAGACCAAUdTdT-3' for knocking down clathrin heavy chain (siCHC), and a negative control (siRNA CR) were purchased from Ribobio (Guangzhou, China). These siRNAs were transfected into HeLa cells using Lipofectamine 2000 according to the manufacturer's instructions. After incubation for 48 h, the cells were harvested, washed twice with PBS, and seeded in 48-well plates with DMEM. FAM-145 nucleosomes were added to the medium (final 20 nM), and incubation was continued for 10 h. The samples were analysed by flow cytometry as described above.

Western blotting

HeLa cells were lysed with RIPA buffer. Whole-cell lysates were collected after centrifugation at 10 000 × g for 15 min at 4°C. Total proteins of cell extracts were assayed using the bicinchoninic acid (BCA) Protein Quantification Kit (Yeasen, Shanghai, China). Forty-microgram protein samples were loaded in each lane of 12% SDS PAGE and transferred to immunoblot PVDF membranes (Millipore). The membrane was probed with anti- β -actin (1:2500), anti-caveolin-1 (1:1000) or anti-CHC (1:1000) rabbit polyclonal antibody and then incubated with horseradish peroxidase-conjugated secondary antibody directed against rabbit IgG (1:4000). After incubation with Western Lightning BeyoECL Plus, the membrane was visualized with a Tanon-5500 Chemiluminescent Imaging System (Tanon Science and Technology, Shanghai, China).

Colocalization assay of FAM-145 nucleosomes with transferrin (Tfn) or cholera toxin subunit B (CTB)

HeLa cells were seeded in 48-well plates. After overnight culture on glass coverslips, FAM-145-nucleosomes (40 nM) together with Cy3-conjugated transferrin (Cy3-Tfn, 75 μ g/ml) or Alexa Fluor 555-conjugated cholera toxin subunit B (AF555-CTB, 1 μ g/ml) were added to the medium. The cells were incubated at 37°C for a certain period of time. The cells were first washed with acidic stripping buffer (0.5 M NaCl, 0.5% acetic acid, pH 3.0) and then with PBS. The cells were fixed in 4% paraformaldehyde (PFA) for 15 min at room temperature. Then, coverslips were mounted on clean glass slides, and image capture was performed by LSCM.

Colocalization assay of FAM-145 nucleosomes with endocytosomes

HeLa cells were seeded in 48-well plates. After culture overnight on glass coverslips, the cells were treated with 100

μ l of Opti-MEM containing nucleosomes (final 40 nM) at 37°C for various times. After two washes with PBS, the cells were fixed in 4% paraformaldehyde for 15 min at room temperature, permeabilized for 10 min in 0.3% (v/v) Triton X-100 and blocked with 5% BSA for 30 min at room temperature. The cells were incubated with anti-EEA1 mouse monoclonal antibody (1:50) overnight at 4°C. The cells were washed twice with PBS and then incubated with DyLight 649 goat anti-mouse IgG (1:80) for 1 h at room temperature, and coverslips were mounted on clean glass slides. Image capture was performed by LSCM.

Colocalization assay of FAM-145 nucleosomes with lysosomes, ER and Golgi

HeLa cells were seeded in 48-well plates. After culture overnight on glass coverslips, the cells were treated with 100 μ l of Opti-MEM containing nucleosomes (final 40 nM) for various times. ER-Tracker Red (1 nM), Golgi-Tracker Red (333 ng/ml), or Lyso-Tracker Red (75 nM) was added to the medium according to the manufacturer's instructions. After the cells were washed with PBS, they were fixed in 4% paraformaldehyde (PFA) for 15 min at room temperature. Then, the fixed cells were washed in PBS and stained with DAPI, and coverslips were mounted on clean glass slides. Image capture was performed by LSCM.

Statistical analysis

We performed statistical analysis by Student's t-test. Significance levels of $P > 0.05$, $0.05 > P > 0.01$, $0.01 > P > 0.001$ and $0.001 > P$ are denoted in graphs by ns, a single, double, or triple asterisk, respectively.

RESULTS

Cellular internalization of nucleosomes through energy-dependent endocytosis

In our previous study, using FAM-145 nucleosomes prepared by complexing 145 bp Widom 601 DNA with histone octamer (22–26), we demonstrated that nucleosomes can be efficiently taken up by all the mammalian cells we examined, including HeLa, HepG2, LO2, THP1, L929 and BMDM cells (20). In the present study, we used FAM-145 nucleosomes and HeLa cells to elucidate the cellular internalization mechanism in detail (Figure 1). The HeLa cell line was chosen because (i) its endocytic machinery has been well characterized and common endocytic pathways are present and (ii) it is one of the most popular cell lines used for endocytosis studies due to experimental tractability (27).

We incubated HeLa cells with 145 nucleosomes containing FAM labelling at the 5'-end of one DNA strand (FAM-145 nucleosome, Figure 1). Flow cytometric analysis revealed that after incubation at 37°C for 6 h, 9% of the cells showed fluorescence (Figure 2A & B), whereas <1% of the control cells showed fluorescence (incubation with FAM-labelled 145 bp dsDNA, FAM-145-dsDNA). FAM-145-nucleosome treatment resulted in a 2-fold increase in the mean fluorescence intensity (MFI, Figure 2C). Confocal fluorescence microscopy analysis of the nucleosome-treated

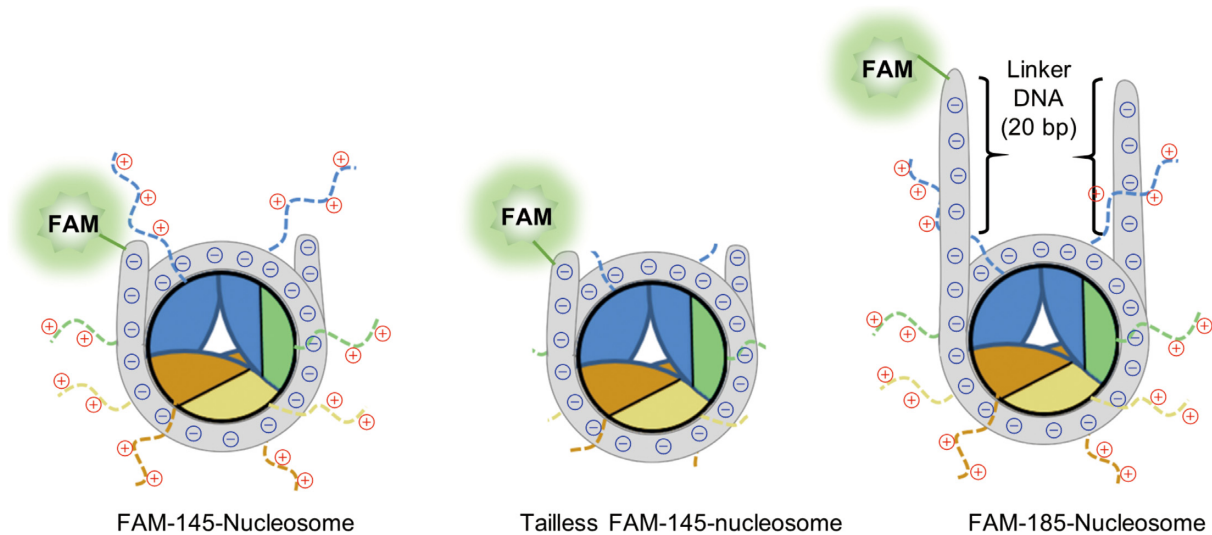


Figure 1. Schematic diagram of the nucleosomes used in the present study.

cells showed that fluorescent spots were located inside cells (Figure 2D). These results are consistent with our previous results and confirm that nucleosomes can be taken up by HeLa cells.

Biomacromolecules are generally taken up by cells via endocytosis, which is energy-dependent and can be inhibited by the presence of NaN_3 or at 4°C (28). We found that both NaN_3 and incubation at 4°C substantially reduced the efficiency of cellular internalization of nucleosomes (Figure 2A–C), indicating that the majority of cellular internalization of nucleosomes involves energy-dependent endocytosis.

The binding of nucleosomes on the cell surface is driven by nonspecific electrostatic interactions

Endocytosis is initiated by the binding of cargoes on the surface of the cytoplasmic membrane, which is followed by an internalization process (29). The binding step, in contrast to the internalization step, is not inhibited by incubation at 4°C (30). We thus incubated HeLa cells with FAM-145 nucleosomes at 4°C for 30 min, and confocal fluorescence microscopy confirmed that nucleosomes converged on the cell surface (Figure 3A). The bound nucleosomes were stripped off by a simple acid wash step (31). In addition, brief treatment of the cells with trypsin before adding nucleosomes substantially prevented nucleosome binding (Figure 3A and B). These results suggest that nucleosomes are recruited to cells by noncovalent interactions with ligands on the cellular surface.

DNA is poorly permeable in the cell membrane, but histones can efficiently enter cells and have been used for gene delivery (18). The potency of histones in gene delivery is highly dependent on their positively charged N-terminal tails (18,32,33). In nucleosomes, the N-terminal tails of histones extrude from the core particle (Figure 1). Thus, it is reasonable to assume that the N-terminal tails are the driving force of nucleosome binding on the cell membrane. To test this hypothesis, we prepared tailless FAM-145 nucleosomes

in which four wild-type histones were replaced by tailless histone mutants (Figure 1) (34). Absorption of tailless FAM-145 nucleosomes on HeLa cells at 4°C was dramatically suppressed relative to that of wild-type FAM-145 nucleosomes (Figure 3C and D), confirming that histone N-terminal tails play a major role in interactions with ligands on the cell surface.

In general, recruitment of cargoes on the cell surface proceeds either by selective interaction with specific receptors or by nonselective interactions, such as hydrophobic and electrostatic interactions, with nonspecific ligands on the cell surface (27). To determine by which type of interaction the histone N-terminal tails bind on the cell surface, we prepared FAM-185 nucleosomes by introducing 20 bp linker DNA at both ends of FAM-145 nucleosomes (Figure 1). FAM-145 nucleosomes and FAM-185 nucleosomes have the same histone octamer. If selective interaction between histone N-terminal tails and specific receptors is the predominant driving force for the binding of nucleosomes on the cell surface, similar binding efficiency would be observed for FAM-145 nucleosomes and FAM-185 nucleosomes. However, the level of FAM-185-nucleosome binding was only 40% that of FAM-145-nucleosome binding. Therefore, it seems that nonselective electrostatic interactions between the positively charged N-terminal tails and negatively charged ligands on the cell surface are the main drivers of nucleosome recruitment on the cell surface.

The Lys (K) to Arg (R) mutation changes the composition of histones but retains the overall charge under physiological conditions (21). To further verify the key role of electrostatic interactions on the binding of nucleosomes to the cellular surface, we prepared four histone mutants in which all Lys residues in the N-terminal tails were mutated to Arg (Figure 4A). Folding of histone octamers using the four histone mutants resulted in precipitation, precluding the preparation of nucleosomes containing four K/R mutated histones. Fortunately, 145 FAM nucleosomes containing two histone mutants, the H3-K/R mutant and the

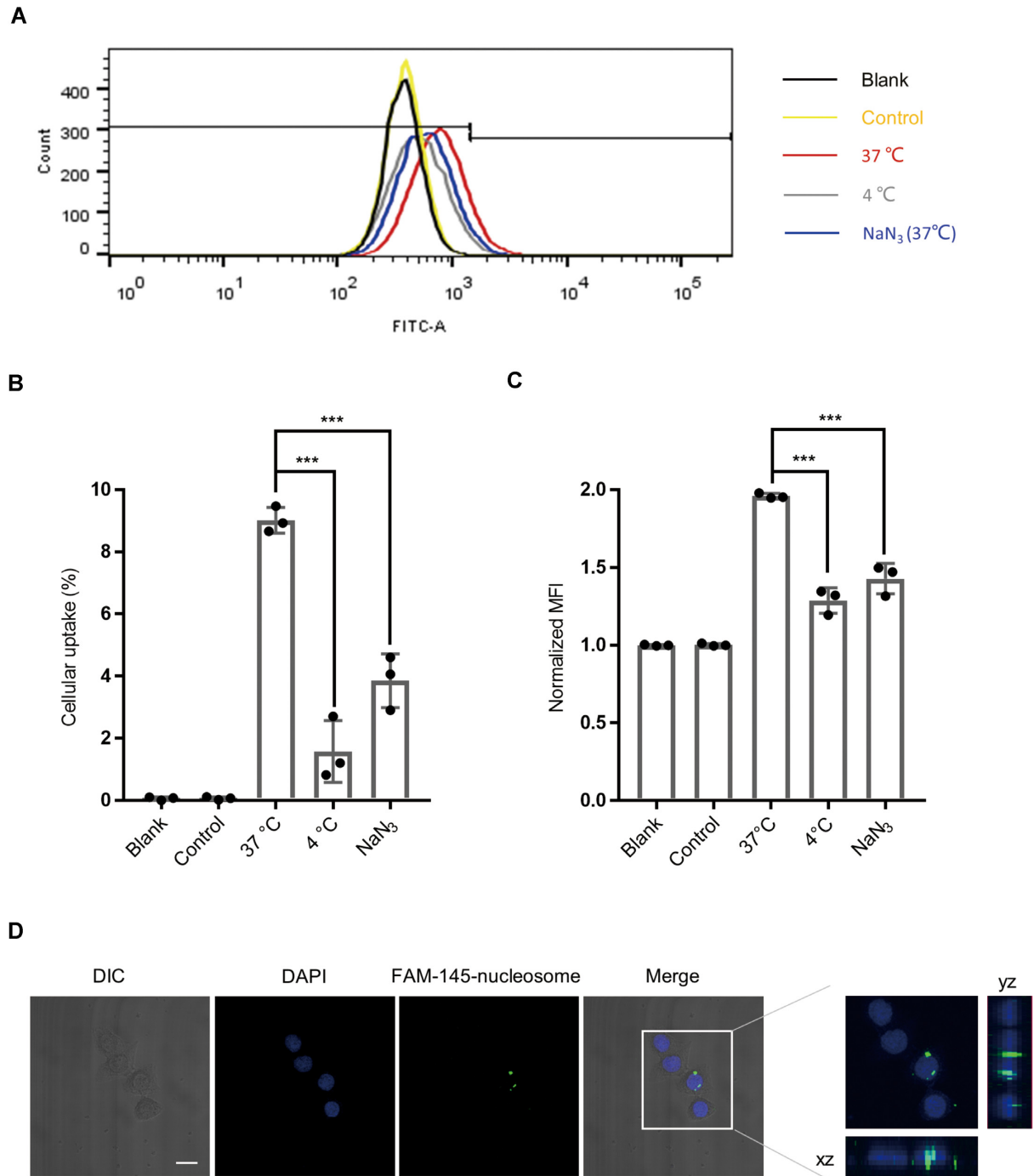


Figure 2. Cellular uptake of nucleosomes occurs by energy-dependent endocytosis. (A) Flow cytometric analysis of HeLa cells after incubation with FAM-145 nucleosomes (20 nM) under different conditions for 6 h. Quantitative results are shown in panels (B) and (C). Control, incubation of HeLa cells with FAM-145-dsDNA. MFI, mean fluorescence intensity. (D) Representative images showing the cellular location of FAM-145 nucleosomes in HeLa cells after incubation for 6 h. Scale bar, 20 μ m. Error bars indicate the mean \pm standard deviation of at least three independent experiments. Statistical significance was determined based on Student's *t*-test (ns, $P > 0.05$; * $0.05 > P > 0.01$; ** $0.01 > P > 0.001$; *** $0.001 > P$).

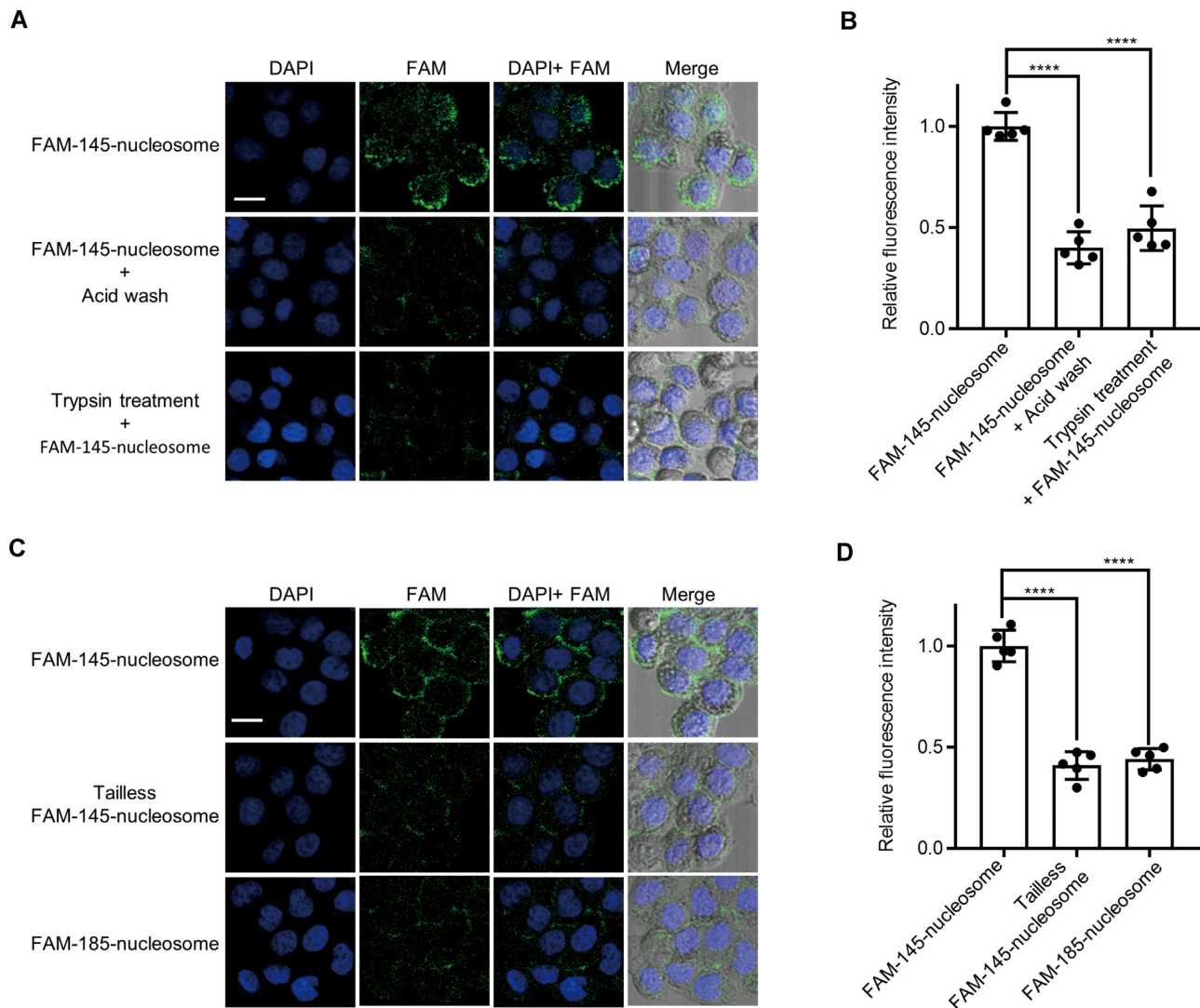


Figure 3. Confocal fluorescence microscopy analyses of the binding of nucleosomes on the HeLa cell surface after incubation at 4°C for 30 min. (A) Representative images showing the binding of FAM-145 nucleosomes on the HeLa cell surface after different treatments. An acid wash of HeLa cells was applied after incubation with 145 nucleosomes. Trypsin treatment of HeLa cells was applied before incubation with 145 nucleosomes. The relative FAM fluorescence intensity is compared in panel (B). (C) Representative images showing the binding of different types of nucleosomes on the HeLa cell surface. The relative FAM fluorescence intensity is compared in panel (D). Scale bar, 20 μ m. Error bars indicate the mean \pm standard deviation of at least three independent experiments. Statistical significance was determined based on Student's *t*-test (ns, $P > 0.05$; * $0.05 > P > 0.01$; ** $0.01 > P > 0.001$; *** $0.001 > P$).

H4-K/R mutant (FAM-145-nucleosome-H3,H4-K/R MUT) or the H2A-K/R mutant and the H2B-K/R mutant (FAM-145-nucleosome-H3,H4-K/R MUT), were successfully prepared (Supplementary Figure S1D). The binding of these two K/R mutated nucleosomes on the HeLa cell surface at 4°C was similar to the binding of WT FMA-145 nucleosomes (Figure 4B and C). Flow cytometric analysis revealed that after incubation at 37°C for 6 h, these K/R-mutated FAM-145 nucleosomes were taken up by HeLa cells as efficiently as WT FAM-145 nucleosomes (Figure 4D and E). Collectively, these results confirm that the binding of nucleosomes on the cell surface proceeds mainly by electrostatic interactions between histone N-terminal tails and nonspecific ligands on the cell surface.

Endocytosis of nucleosomes is clathrin- and caveolae-dependent

After binding on the cell surface, cargos undergo endocytic internalization via many different mechanisms, such as clathrin-dependent endocytosis, caveolin-dependent endocytosis, and macropinocytosis. We thus treated HeLa cells with FAM-145 nucleosomes together with various chemical inhibitors of endocytosis, including dynasore and sucrose (inhibitors of clathrin-dependent endocytosis), genistein (GE) and methyl- β -cyclodextrin (M β CD) (inhibitors of caveolin-dependent endocytosis), and ethylisopropylamiloride (EIPA, an inhibitor of macropinocytosis) (35,36). The internalization of nucleosomes was significantly inhibited by dynasore, sucrose, GE and M β CD but was not affected by EIPA (Figure 5A and B and

A

H3-WT: N- ARTKQTARKSTGGKAPRKQLATKAARKSAPATGGVKK-
H3-K/R MUT: N- ARTRQTARRSTGGRAPRRQLATRAARRSAPATGGVRR-

H4-WT: N- SGRGKGGKGLGKGGAKRHRK-
H4-K/R MUT: N- SGRGRGGKGLGRGGARRHRR-

H2A-WT: N- SGRGKQGGKTRAKAK-
H2A-K/R MUT: N- SGRGRQGGKTRARAR-

H2B-WT: N- AKSAPAPKKGSKKAVTKTQKKDGKKRRKTRK-
H2B-K/R MUT: N- ARSAPAPRRGSRRAVTRTQRRDGRRRRRRTRR-

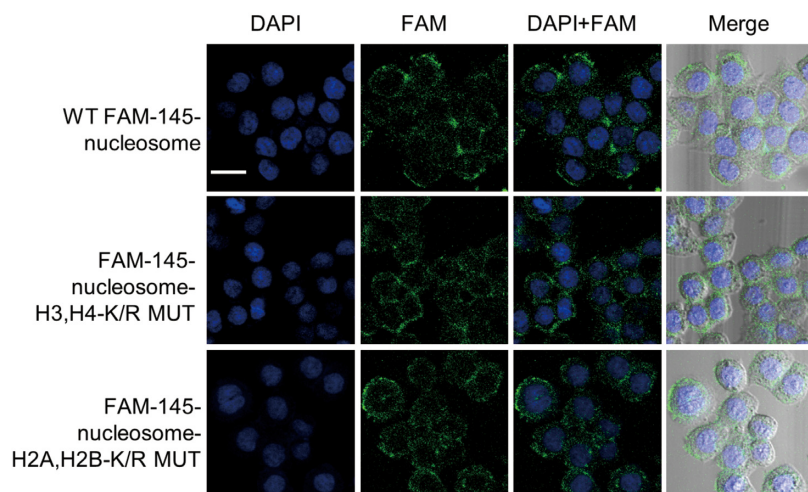
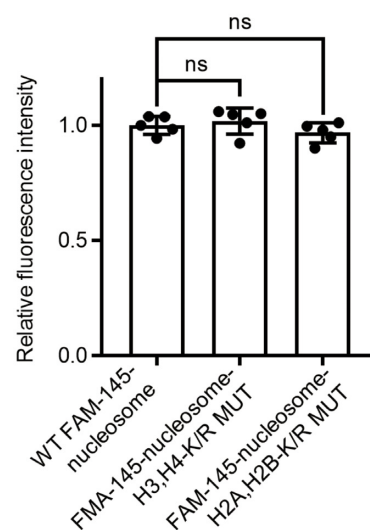
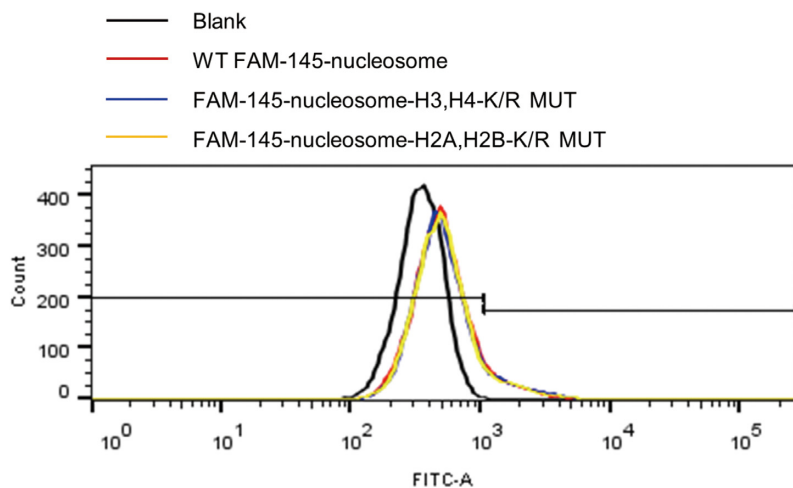
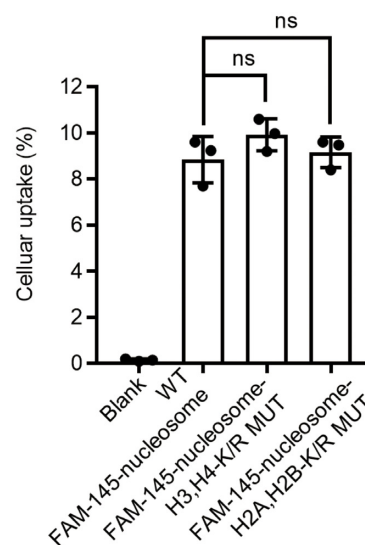
B**C****D****E**

Figure 4. Binding and cellular uptake of K/R-mutated 145-FAM nucleosomes in HeLa cells. **(A)** The sequences of wild-type (WT) and K/R mutated histones. In the mutated histones, all Lys residues in the N-terminal tails are mutated to Arg. **(B)** Representative images showing the binding of WT and K/R mutated 145-FAM nucleosomes on the HeLa cell surface at 4°C for 30 min. Scale bar, 20 μm. The relative FAM fluorescence intensity is compared in panel **(C)**. **(D)** Flow cytometric analysis of HeLa cells after incubation with WT and mutated FAM-145 nucleosomes (20 nM) for 6 h. Quantitative results are shown in panel **(E)**. Error bars indicate the mean ± standard deviation of at least three independent experiments. Statistical significance was determined based on Student's *t*-test (ns, $P > 0.05$; $*0.05 > P > 0.01$; $**0.01 > P > 0.001$; $***0.001 > P$).

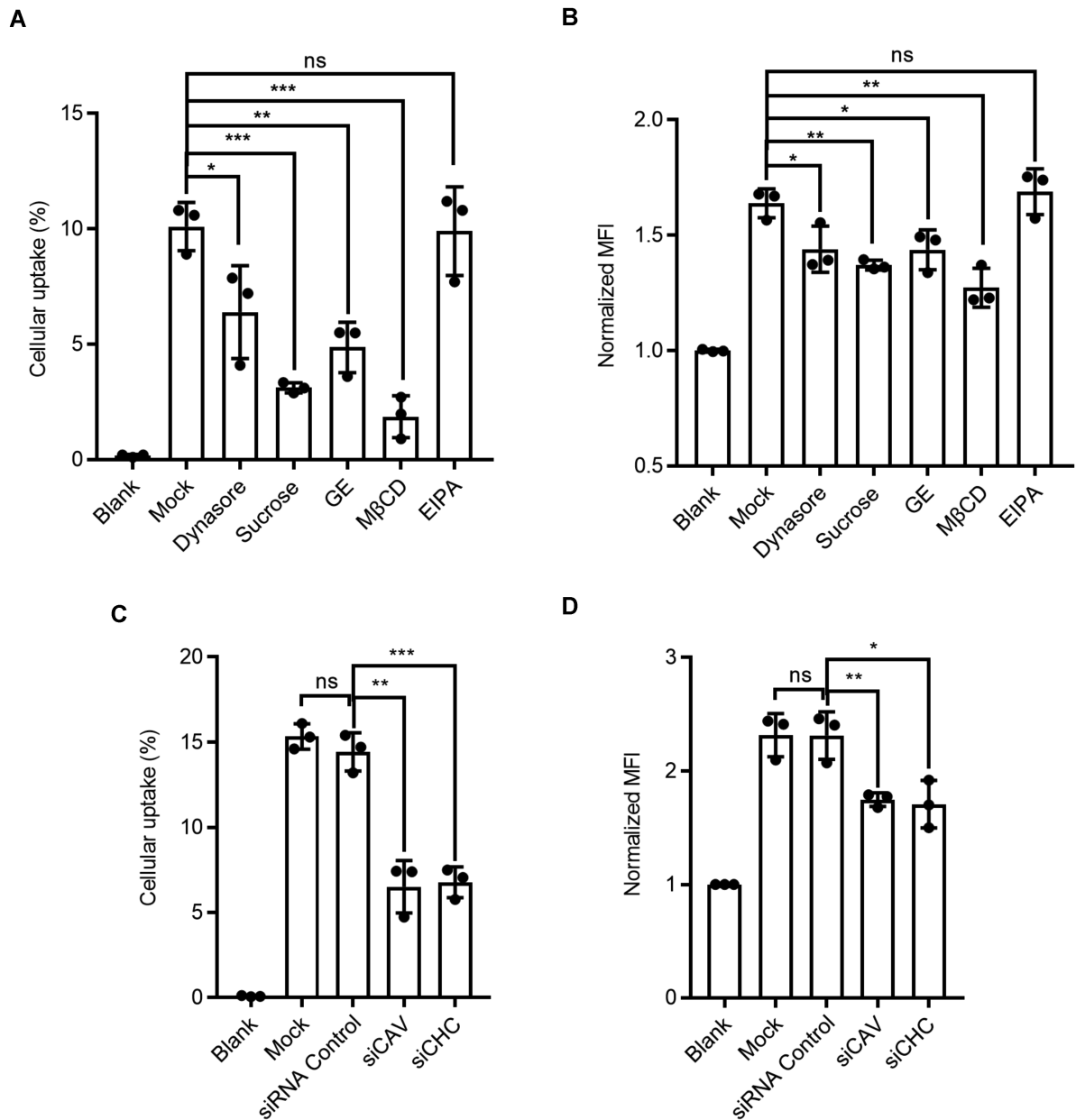


Figure 5. Flow cytometric analysis of cellular uptake of FAM-145 nucleosomes by HeLa cells in the presence of different inhibitors. (A, B) In the presence of chemical endocytosis inhibitors. (C, D) Knockdown of CHC and CAV by siRNA. MFI, mean fluorescence intensity. Error bars indicate the mean \pm standard deviation of at least three independent experiments. Statistical significance was determined based on Student's *t*-test (ns, $P > 0.05$; * $0.05 > P > 0.01$; ** $0.01 > P > 0.001$; *** $0.001 > P$).

Supplementary Figure S2), suggesting that endocytosis of nucleosomes is likely to follow clathrin- and caveolin-dependent pathways.

Clathrin- and caveolin-dependent endocytosis is regulated by clathrin heavy chain (CHC) and caveolin-1 (Cav-1), respectively, and thus can be inhibited by the RNA silencing of CHC (siCHC) and Cav-1 (siCAV) (37). We found that siCHC and siCAV suppressed the cellular uptake of FAM-145 nucleosomes by $\sim 50\%$ (Figure 5C and D and Supplementary Figure S2).

Transferrin (Tfn) and cholera toxin subunit B (CTB) are two well-established endocytic markers that are taken

up by cells via clathrin-mediated endocytosis and caveolin-mediated endocytosis, respectively (38). As a control experiment, we verified the clathrin-dependent endocytosis of Cy3-labeled Tfn (Cy3-Tfn) and caveolin-dependent endocytosis of Alexa Fluor 555-labeled CTB (AF555-CTB) by siRNA inhibition (Supplementary Figure S3). Next, the time-dependent cellular distribution of FAM-145 nucleosomes was studied with Cy3-Tfn and AF555-CTB as references. After treatment of HeLa cells with FAM-145 nucleosomes together with either Cy3-Tfn or AF555-CTB for 20 min, the medium was changed, and culturing was continued. The cellular distribution of FAM-145 nucleosomes,

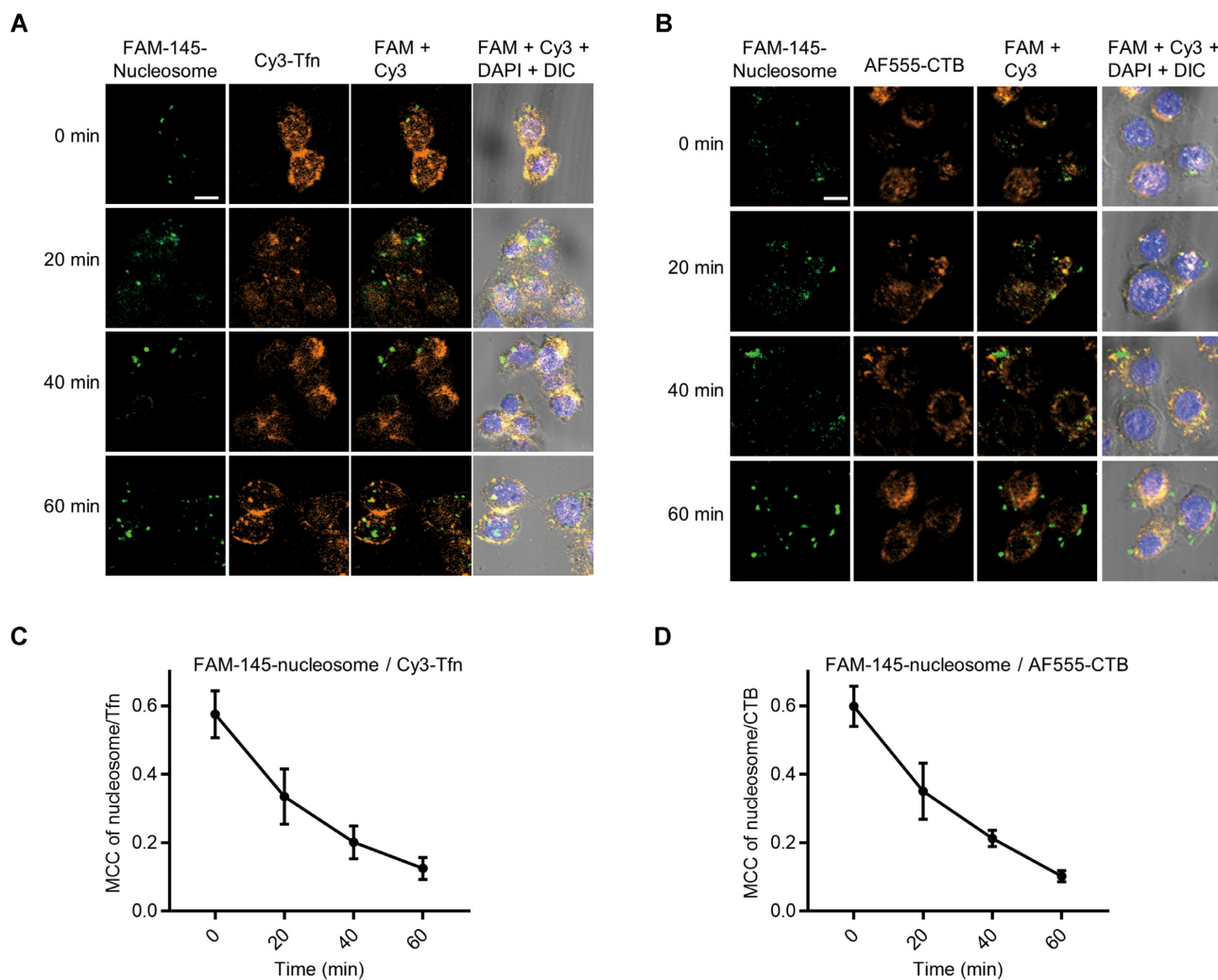


Figure 6. Time-dependent colocalization of FAM-145 nucleosomes with Cy3-Tfn and AF555-CTB in HeLa cells. (A) Confocal microscopy analysis of the colocalization of FAM-145 nucleosomes with Cy3-Tfn. The time-dependent MCC of FAM-145 nucleosomes/Cy3-Tfn is shown in panel (C). (B) Confocal microscopy analysis of the colocalization of FAM-145 nucleosomes with AF555-CTB. The time-dependent MCC of FAM-145 nucleosomes/AF555-CTB is shown in panel (D). For all graphs, error bars indicate the mean \pm standard deviation of at least three independent experiments. Scale bar, 20 μ m.

Cy3-Tfn and AF555-CTB was monitored by confocal fluorescence microscopy at different time points (Figure 6A and B), and the level of colocalization between the two fluorophores was determined according to Manders' colocalization coefficient (MCC). Initially, 58% and 60% of the FAM-145 nucleosomes were colocalized with Cy3-Tfn and AF555-CTB, respectively. The colocalization percentages gradually decreased with the extension of incubation time (Figure 6C and D). Taken together, these results indicated that some nucleosomes were internalized together with Tfn via clathrin-dependent endocytosis and that others were taken up together with CTB through caveolin-mediated endocytosis.

Nucleosomes escape quickly from endosomes

For both clathrin- and caveolin-dependent endocytosis, cargoes are first transported to early endosomes, followed by different intracellular trafficking. Early endosomes may tar-

get lysosomes, and ultimately, the contents are degraded or fused with specific cellular organelles, such as the endoplasmic reticulum (ER) and Golgi apparatus. Some cargoes have the capacity to overcome endosomal entrapment and achieve cytosolic delivery (39).

Next, the intracellular trafficking of endocytic FAM-145 nucleosomes was explored by confocal fluorescence microscopy. After HeLa cells were cultured in the presence of FAM-145 nucleosomes for 20 min, extracellular nucleosomes were washed away, and the culture was continued with fresh medium. The cells were fixed at different time points followed by staining with DyLight 649-labeled antibody against early endosome antigen 1 (EEA1). MCC analyses of the FAM-145 nucleosomes with EEA1 confirmed that nucleosomes were first entrapped in endosomes after initial internalization (MCC = 0.82 ± 0.04 , Figure 7A and Supplementary Figure S4). With the extension of incubation time, the MCC values decreased gradually. After 60 min, only 12% of the nucleosomes were still colocalized with EEA1 (endosomes).

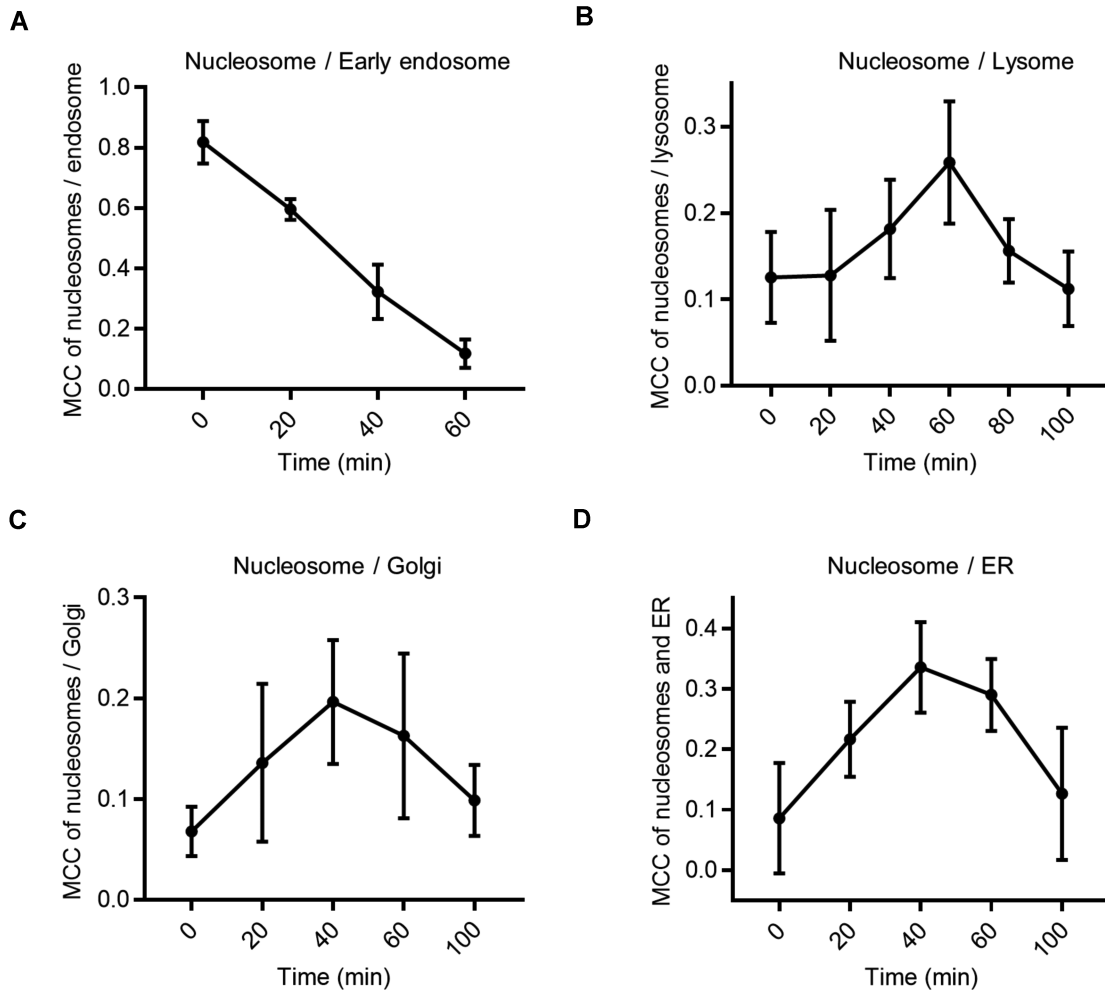


Figure 7. Time-dependent entrapment of FAM-145 nucleosomes in different cell compartments and cellular organelles after endocytosis. (A) MCC of FAM-145 nucleosomes and early endosome antigen 1 (EEA1). (B) MCC of FAM-145 nucleosomes and Lyso-Tracker Red. (C) MCC of FAM-145 nucleosomes and Golgi-Tracker Red. (D) MCC of FAM-145 nucleosomes and ER-Tracker Red. Error bars indicate the mean \pm standard deviation of at least three independent experiments.

Following endosome escape, translocation of nucleosomes into lysosomes, the ER and the Golgi apparatus was observed. Entrapment of nucleosomes in these cellular organelles increased slightly with time, reached a maximum (MCC = 0.2–0.3) at 40–60 min, and then decreased to negligible levels at 100 min (Figure 7B–D and Supplementary Figures S5–S7). These results suggest that targeting endosome-entrapped nucleosomes to multiple cellular organelles occurs to some extent, and these translocations facilitate the escape of nucleosomes.

To determine the longer-term translocation and structural integrity of internalized nucleosomes, we prepared FAM- and Cy3- dual fluorescence-labelled nucleosomes (FAM-Cy3-145-nucleosomes) by treating FAM-145-nucleosomes with Cy3-NHS ester (Figure 8A). Cy3-NHS ester selectively reacts with accessible lysine residues on histones (40). The amount of Cy3-NHS ester was carefully controlled, which allowed us to obtain nucleosomes with limited Cy3 tags attached on any one or several histones. The structural integrity of the obtained FAM-Cy3-145

nucleosomes was confirmed by 1.5% agarose gel analysis (Figure 8B). DNase I footprinting assays showed that FAM-Cy3-145 nucleosomes had the same cleavage pattern as FAM-145 nucleosomes (Supplementary Figure S8), suggesting that Cy3 modifications cause negligible structural disturbance to nucleosomes. After incubation of HeLa cells with FAM-Cy3-145 nucleosomes for 1 h, extracellular nucleosomes were washed away, and incubation was continued with fresh medium. Confocal fluorescence microscopy analyses showed that FAM and Cy3 were mainly distributed in the cytoplasm up to 12 h (Figure 8C). The MCCs of FAM/Cy3 and Cy3/FAM were 0.9 and 0.8, respectively, at the beginning and slightly decreased to 0.8 and 0.6 at 12 h (Figure 8D and Supplementary Figure S9). Therefore, degradation and/or disassembly of nucleosomes in the cytoplasm seems marginal for a rather long time after their rapid escape from different cellular organelles. Of note, we could not rule out the possibility that Cy3 and FAM remain colocalized after nucleosome degradation.

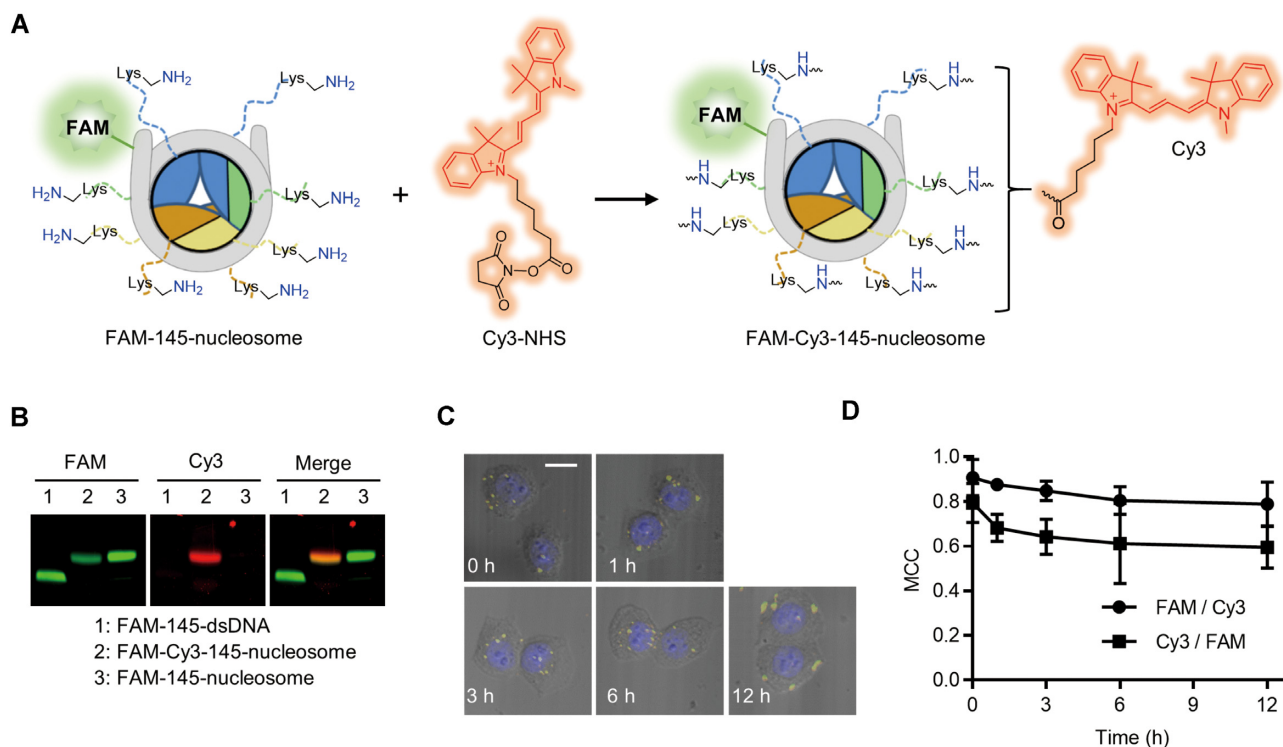


Figure 8. Internalized nucleosomes maintain structural integrity after endosomal escape. (A) Preparation of FAM-Cy3-145-nucleosomes. (B) Agarose gel (1.5%) analysis of the structural integrity of FAM-Cy3-145 nucleosomes. (C) Confocal microscopy analysis of the intracellular distribution of FAM-Cy3-145 nucleosomes after incubation for 12 h. Scale bar, 20 μm . (D) The time-dependent MCC of FAM/Cy3 and Cy3/FAM. Error bars indicate the mean \pm standard deviation of at least three independent experiments.

Endocytosis of nucleosomes by THP1 cells

We have demonstrated that except for HeLa cells, a broad range of mammalian cell lines can take up nucleosomes, and the uptake efficiency varies in different cell lines (20). This finding indicates that endocytosis of nucleosomes in different cell lines may follow different pathways. Given the potential linkage between circulating nucleosomes and immunostimulation, we investigated the endocytic mechanism of nucleosomes by a monocyte- and macrophage-like cell line, THP1. THP1 is an immortalized cell line resembling primary monocytes and macrophages in morphological and functional properties and has been widely used to study immune responses (41).

Flow cytometric analysis of the cellular uptake of FAM-145 nucleosomes by THP1 cells revealed that the internalization of nucleosomes was significantly inhibited by dynasore and sucrose but not by GE and EIPA (Figure 9A and Supplementary Figure S10A). In addition, we found that siCHC but not siCAV suppressed the cellular uptake of 145-FAM nucleosomes by THP1 cells (Figure 9B and Supplementary Figure S10B and C). These results indicate that endocytosis of nucleosomes by THP1 cells mainly involves the clathrin-dependent pathway, and the caveolin-dependent pathway is not included. This finding is consistent with the fact that THP-1 cells weakly express caveolin-1; thus, caveolin-dependent endocytosis is absent (42). Notably, endocytosis of nucleosomes by THP1 cells was also inhibited by M β CD, which is known to inhibit caveolin-mediated endocytosis and lipid raft formation. Therefore,

some other endocytic pathways, e.g., lipid raft-dependent pathways, may be involved in the internalization of nucleosomes in THP1 cells.

DISCUSSION

In this study, we studied the cellular entry mechanism of nucleosomes using reconstituted nucleosomes and HeLa cells. We demonstrated that extracellular nucleosomes can be absorbed on the cytoplasmic membrane and that this absorption is driven by nonspecific electrostatic interactions between the positively charged histone N-terminal tails and the negatively charged ligands on the cell surface. Internalization of adsorbed nucleosomes proceeds by clathrin- and caveolae-dependent endocytosis, transporting nucleosomes into endosomes. Rapid endosomal escape leads to the release of nucleosomes into the cytosol, where nucleosomes remain intact for an extended period.

Nanoparticles facilitate endocytosis and have been extensively used in cargo delivery into cells (27). The cellular uptake efficiency and endocytic mechanism of nanoparticles are affected by their physicochemical properties, such as size, surface charge and surface hydrophobicity/hydrophilicity (43). In general, large nanoparticles (>0.2 μm) are taken up by cells via macropinocytosis, and small nanoparticles achieve cellular entry by clathrin- and caveolae-dependent endocytosis. Endocytosis of positively charged nanoparticles is generally more efficient than endocytosis of zwitterionic and anionic nanoparticles (29,44). Nucleosomes are nanoparticles with

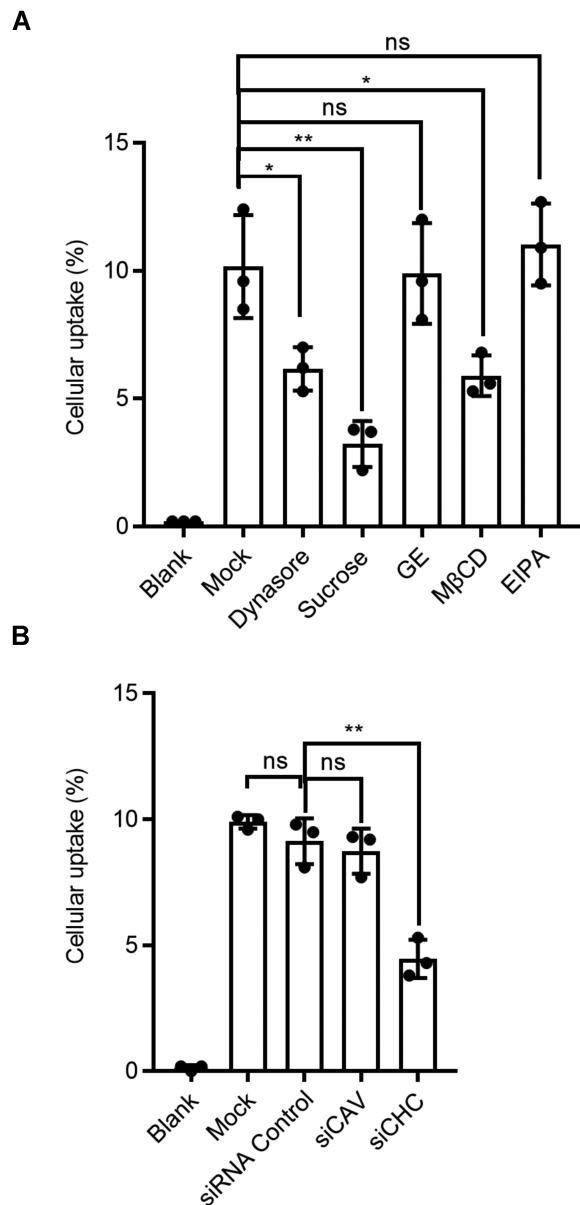


Figure 9. Flow cytometric analysis of the cellular uptake of FAM-145 nucleosomes by THP1 cells in the presence of different inhibitors. (A) Chemical endocytosis inhibitors. (B) Knockdown of CHC and CAV by siRNA. Error bars indicate the mean \pm standard deviation of at least three independent experiments. Statistical significance was determined based on Student's *t*-test (ns, $P > 0.05$; $*0.05 > P > 0.01$; $**0.01 > P > 0.001$; $***0.001 > P$).

a diameter of 11 nm. The small size of nucleosomes is favourable for clathrin- and caveolae-dependent endocytosis but unfavourable for macropinocytosis. Regarding the charge, the nucleosome is zwitterionic, and the total number of anions slightly exceeds the number of cations. However, the distribution patterns of anions and cations in nucleosomes are different. Anions contributed by the phosphate linkage of DNA are evenly distributed on the outer surface of the nucleosomes, whereas cations contributed by the positively charged Lys and Arg residues are mainly located at the N-terminal tails of histones that extrude

from the nanoparticle (Figure 1). As a result, the positively charged N-terminal tails of histones are more readily available for electrostatic interaction with the negatively charged cell membrane, which facilitates the absorption of nucleosomes on the cell surface and subsequent internalization via endocytosis. Collectively, the small particle size and the unique charge distribution pattern render nucleosomes prone to clathrin- and caveolin-dependent endocytosis.

The time-dependent study of colocalization between nucleosomes and different cell compartments after internalization revealed that nucleosomes rapidly escaped from the endosomes, lysosomes, ER and Golgi apparatus. In addition, in our previous study, we demonstrated that after cellular entry, nucleosomes are bound by cGAS, a pattern recognition receptor in the cytosol. Collectively, we can conclude that after cellular internalization, nucleosomes rapidly escape from endosomes and are released into the cytosol.

Arg-rich polycationic peptides have been extensively used in cellular delivery and show promising endosomal escape through different mechanisms, such as vesicle collapse and membrane destabilization effects (39,45). In this regard, it is reasonable to attribute the rapid endosome escape of nucleosomes to the Lys- and Arg-rich, polycationic N-terminal tails of histones. Although the exact mechanism of endosomal escape after nucleosome endocytosis remains to be addressed in the future, it is clear that assembly of anionic polymers with cationic peptides in a pattern similar to that in nucleosomes facilitates endocytosis and rapid endosomal escape. This strategy may be invaluable for constructing nanoparticles for efficient delivery of therapeutic oligonucleotides and genes.

Due to the weak expression of caveolin-1 in THP1 cells, caveolin-dependent endocytosis of nucleosomes was absent, and clathrin-dependent endocytosis was the main pathway. In addition, the possibility of clathrin/caveolin-independent endocytosis, such as the lipid raft-dependent pathway, cannot be ruled out in THP1 cells. Thus, the cellular entry of nucleosomes into immune cells seems to follow slightly different endocytic machinery than into epithelial cells. Of note, although THP1 cells resemble primary monocytes and macrophages in morphological and functional properties, they are not primary cells. The mechanism in primary cells remains to be validated in the future.

In conclusion, we demonstrated that extracellular nucleosomes can be taken up by various cell lines through multiple endocytic pathways. These results suggest that trafficking of circulating nucleosomes into different kinds of somatic cells is a common phenomenon that may lead to diverse biological consequences. Apoptosis is a major source of circulating nucleosomes. Thus, circulating nucleosomes may contain mutated genes and aberrant DNA/histone modifications, making them structurally different than host nucleosomes. Internalized circulating nucleosomes in immune cells may be recognized as pathogen-associated molecular patterns or damage-associated molecular patterns triggering the immune response. This phenomenon provides a reasonable explanation for the linkage between circulating nucleosomes and systemic autoimmune diseases. In addition, endocytosis of circulating nucleosomes by somatic cells

represents an efficient approach for translocation of pathogenic genes into normal cells. Expression of the pathogenic genes or homologous recombination of the pathogenic genes into the host genome may lead to cellular disorders. Thus, a considerable amount of work remains to be conducted to further explore the biological consequences of endocytic nucleosomes.

DATA AVAILABILITY

Flow cytometry datasets have been deposited in FlowRepository (<http://flowrepository.org/>) with Repository FR-FCM-Z3KJ, FR-FCM-Z459, FR-FCM-Z45E, FR-FCM-Z45C, FR-FCM-Z45F, FR-FCM-Z45G.

SUPPLEMENTARY DATA

Supplementary Data are available at NAR Online.

FUNDING

Natural Science Foundation of China [21877064, 91953115]; Natural Science Foundation of Tianjin City [20JCZDJC00830]; Frontiers Science Center for New Organic Matter, Nankai University [63181206]. Funding for open access charge: Natural Science Foundation of China.

Conflict of interest statement. None declared.

REFERENCES

- McGinty, R.K. and Tan, S. (2015) Nucleosome structure and function. *Chem. Rev.*, **115**, 2255–2273.
- Holdenrieder, S., Stieber, P., Bodenmuller, H., Busch, M., Pawel, J., Schalhorn, A., Nagel, D. and Seidel, D. (2001) Circulating nucleosomes in serum. *Ann. N. Y. Acad. Sci.*, **945**, 93–102.
- Rahier, J.-F., Druetz, A., Faugeras, L., Martinet, J.-P., Géhénot, M., Josseaux, E., Herzog, M., Micallef, J., George, F., Delos, M. *et al.* (2017) Circulating nucleosomes as new blood-based biomarkers for detection of colorectal cancer. *Clin. Epigenet.*, **9**, 53.
- Hayakawa, M., Ooyasu, T., Sadamoto, Y., Saito, T., Yoshida, T., Katabami, K., Wada, T., Maekawa, K. and Ieko, M. (2020) Microparticles and nucleosomes are released from parenchymal cells destroyed after injury in a rat model of blunt trauma. *Clin. Appl. Thromb.-Hem.*, <https://doi.org/10.1177/1076029620950825>.
- Marsman, G., Zeerleder, S. and Luken, B.M. (2016) Extracellular histones, cell-free DNA, or nucleosomes: differences in immunostimulation. *Cell Death Dis.*, **7**, e2518.
- Mackenzie, K.J., Carroll, P., Martin, C.A., Murina, O., Fluteau, A., Simpson, D.J., Olova, N., Sutcliffe, H., Rainger, J.K., Leitch, A. *et al.* (2017) cGAS surveillance of micronuclei links genome instability to innate immunity. *Nature*, **548**, 461–465.
- Zierhut, C., Yamaguchi, N., Paredes, M., Luo, J.D., Carroll, T. and Funabiki, H. (2019) The cytoplasmic DNA sensor cGAS promotes mitotic cell death. *Cell*, **178**, 302–315.
- Boyer, J.A., Spangler, C.J., Strauss, J.D., Cesmat, A.P., Liu, P., McGinty, R.K. and Zhang, Q. (2020) Structural basis of nucleosome-dependent cGAS inhibition. *Science*, **370**, 450–454.
- Kujirai, T., Zierhut, C., Takizawa, Y., Kim, R., Negishi, L., Uruma, N., Hirai, S., Funabiki, H. and Kurumizaka, H. (2020) Structural basis for the inhibition of cGAS by nucleosomes. *Science*, **370**, 455–458.
- Michalski, S., de Oliveira Mann, C.C., Stafford, C., Witte, G., Bartho, J., Lammens, K., Hornung, V. and Hopfner, K.-P. (2020) Structural basis for sequestration and autoinhibition of cGAS by chromatin. *Nature*, **587**, 678–682.
- Pathare, G.R., Decout, A., Glück, S., Cavadini, S., Makasheva, K., Hovius, R., Kempf, G., Weiss, J., Kozicka, Z., Guey, B. *et al.* (2020) Structural mechanism of cGAS inhibition by the nucleosome. *Nature*, **587**, 668–672.
- Zhao, B., Xu, P., Rowlett, C.M., Jing, T., Shinde, O., Lei, Y., West, A.P., Liu, W.R. and Li, P. (2020) The molecular basis of tight nuclear tethering and inactivation of cGAS. *Nature*, **587**, 673–677.
- Sun, L., Wu, J., Du, F., Chen, X. and Chen, Z.J. (2013) Cyclic GMP-AMP synthase is a cytosolic DNA sensor that activates the type I interferon pathway. *Science*, **339**, 786–791.
- Ablasser, A. and Chen, Z.J. (2019) cGAS in action: Expanding roles in immunity and inflammation. *Science*, **363**, eaat8657.
- Roberts, T.C., Langer, R. and Wood, M.J.A. (2020) Advances in oligonucleotide drug delivery. *Nat. Rev. Drug Discov.*, **19**, 673–694.
- Juliano, R.L. (2016) The delivery of therapeutic oligonucleotides. *Nucleic Acids Res.*, **44**, 6518–6548.
- Rosenbluh, J., Hariton-Gazal, E., Dagan, A., Rottem, S., Graessmann, A. and Loyer, A. (2005) Translocation of histone proteins across lipid bilayers and mycoplasma membranes. *J. Mol. Biol.*, **345**, 387–400.
- Kaouass, M., Beaulieu, R. and Balicki, D. (2006) Histonefection: Novel and potent non-viral gene delivery. *J. Controlled Release*, **113**, 245–254.
- Mosquera, J., García, I. and Liz-Marzán, L.M. (2018) Cellular uptake of nanoparticles versus small molecules: A matter of size. *Acc. Chem. Res.*, **51**, 2305–2313.
- Wang, H., Zang, C., Ren, M., Shang, M., Wang, Z., Peng, X., Zhang, Q., Wen, X., Xi, Z. and Zhou, C. (2020) Cellular uptake of extracellular nucleosomes induces innate immune responses by binding and activating cGMP-AMP synthase (cGAS). *Sci. Rep.*, **10**, 15385.
- Szczepanski, J.T., Zhou, C.Z. and Greenberg, M.M. (2013) Nucleosome core particle-catalyzed strand scission at abasic sites. *Biochemistry*, **52**, 2157–2164.
- Vasudevan, D., Chua, E.Y.D. and Davey, C.A. (2010) Crystal structures of nucleosome core particles containing the ‘601’ strong positioning sequence. *J. Mol. Biol.*, **403**, 1–10.
- Ren, M., Shang, M., Wang, H., Xi, Z. and Zhou, C. (2021) Histones participate in base excision repair of 8-oxodGuo by transiently cross-linking with active repair intermediates in nucleosome core particles. *Nucleic Acids Res.*, **49**, 257–268.
- Ren, M., Cheng, Y., Duan, Q. and Zhou, C. (2019) Transesterification reaction and the repair of embedded ribonucleotides in DNA are suppressed upon the assembly of DNA into nucleosome core particles. *Chem. Res. Toxicol.*, **32**, 926–934.
- Ren, M., Bai, J., Xi, Z. and Zhou, C. (2019) DNA damage in nucleosomes. *Sci. China Chem.*, **62**, 561–570.
- Li, F., Zhang, Y., Bai, J., Greenberg, M.M., Xi, Z. and Zhou, C. (2017) 5-formylcytosine yields DNA–protein cross-links in nucleosome core particles. *J. Am. Chem. Soc.*, **139**, 10617–10620.
- Behzadi, S., Serpooshan, V., Tao, W., Hamaly, M.A., Alkawareek, M.Y., Dreaden, E.C., Brown, D., Alkilany, A.M., Farokhzad, O.C. and Mahmoudi, M. (2017) Cellular uptake of nanoparticles: Journey inside the cell. *Chem. Soc. Rev.*, **46**, 4218–4244.
- Doherty, G.J. and McMahon, H.T. (2009) Mechanisms of endocytosis. *Annu. Rev. Biochem.*, **78**, 857–902.
- Cho, E.C., Xie, J., Wurm, P.A. and Xia, Y. (2009) Understanding the role of surface charges in cellular adsorption versus internalization by selectively removing gold nanoparticles on the cell surface with a I₂/KI etchant. *Nano Lett.*, **9**, 1080–1084.
- Sato, K., Nagai, J., Mitsui, N., Ryoko, Y. and Takano, M. (2009) Effects of endocytosis inhibitors on internalization of human IgG by Caco-2 human intestinal epithelial cells. *Life Sci.*, **85**, 800–807.
- Kameyama, S., Horie, M., Kikuchi, T., Omura, T., Tadokoro, A., Takeuchi, T., Nakase, I., Sugiura, Y. and Futaki, S. (2007) Acid wash in determining cellular uptake of fab/cell-permeating peptide conjugates. *Biopolymers*, **88**, 98–107.
- Balicki, D., Putnam, C.D., Scaria, P.V. and Beutler, E. (2002) Structure and function correlation in histone H2A peptide-mediated gene transfer. *Proc. Natl. Acad. Sci. U.S.A.*, **99**, 7467–7471.
- Watson, K., Gooderham, N.J., Davies, D.S. and Edwards, R.J. (1999) Nucleosomes bind to cell surface proteoglycans. *J. Biol. Chem.*, **274**, 21707–21713.
- Shang, M., Ren, M. and Zhou, C. (2019) Nitrogen mustard induces formation of DNA–histone cross-links in nucleosome core particles. *Chem. Res. Toxicol.*, **32**, 2517–2525.
- Ivanov, A.I. (2008) In: Ivanov, A.I. (ed). *Exocytosis and Endocytosis*. Humana Press, Totowa, NJ, pp. 15–33.

36. Dutta,D. and Donaldson,J.G. (2012) Search for inhibitors of endocytosis. *Cellular Logistics*, **2**, 203–208.
37. Al Soraj,M., He,L., Peynshaert,K., Cousaert,J., Vercauteren,D., Braeckmans,K., De Smedt,S.C. and Jones,A.T. (2012) siRNA and pharmacological inhibition of endocytic pathways to characterize the differential role of macropinocytosis and the actin cytoskeleton on cellular uptake of dextran and cationic cell penetrating peptides octaarginine (R8) and HIV-Tat. *J. Control. Release*, **161**, 132–141.
38. Missirlis,D. (2014) The effect of substrate elasticity and actomyosin contractility on different forms of endocytosis. *PLoS One*, **9**, e96548.
39. Pei,D. and Buyanova,M. (2019) Overcoming endosomal entrapment in drug delivery. *Bioconjugate Chem.*, **30**, 273–283.
40. Koniev,O. and Wagner,A. (2015) Developments and recent advancements in the field of endogenous amino acid selective bond forming reactions for bioconjugation. *Chem. Soc. Rev.*, **44**, 5495–5551.
41. Chanput,W., Mes,J.J. and Wichers,H.J. (2014) THP-1 cell line: an in vitro cell model for immune modulation approach. *Int. Immunopharmacol.*, **23**, 37–45.
42. Matveev,S., van der Westhuyzen,D.R. and Smart,E.J. (1999) Co-expression of scavenger receptor-bi and caveolin-1 is associated with enhanced selective cholesteryl ester uptake in THP-1 macrophages. *J. Lipid Res.*, **40**, 1647–1654.
43. Ju,Y., Guo,H., Edman,M. and Hamm-Alvarez,S.F. (2020) Application of advances in endocytosis and membrane trafficking to drug delivery. *Adv. Drug Deliv. Rev.*, **157**, 118–141.
44. Jiang,Y., Huo,S., Mizuhara,T., Das,R., Lee,Y.-W., Hou,S., Moyano,D.F., Duncan,B., Liang,X.-J. and Rotello,V.M. (2015) The interplay of size and surface functionality on the cellular uptake of sub-10 nm gold nanoparticles. *Acs Nano*, **9**, 9986–9993.
45. Dougherty,P.G., Sahni,A. and Pei,D. (2019) Understanding cell penetration of cyclic peptides. *Chem. Rev.*, **119**, 10241–10287.